JMEPEG (2010) 19:1199–1204
DOI: 10.1007/s11665-009-9585-5

1059-9495/$19.00

Nonlocal Effects in the Confocal μ-Raman Characterization of Inhomogeneous Polymer Coatings

R. Rodriguez, S. Vargas, and M. Estevez

(Submitted June 8, 2009; in revised form November 11, 2009)

The confocal μ-Raman technique was used to characterize the morphology of inhomogeneous anti-graffiti coatings; for these systems, the antiadherent molecules were segregated to the external (exposed) surface forming a layer whose thickness was determined. The confocal data from these inhomogeneous coatings contains nonlocal contributions because the light scattered from sources near the specific specimen under analysis (the focused region) could not be completely rejected by the spatial filter of the confocal device. These nonlocal contributions had important effects in the Raman spectra, modifying the bands height profiles of homogeneous and inhomogeneous materials allowing their identification. Taking into account these nonlocal effects, it was possible to interpret correctly the relative intensities of the Raman bands and characterize properly the inhomogeneous coatings.

Keywords confocal technique, inhomogeneous coatings characterization, micro-Raman spectroscopy, nonlocal contribution, phase segregation

1. Introduction

The confocal technique represents an important advance in optical microscopy because enables visualization deep into the sample allowing observation and analysis of sharply defined sections from which it is possible generate, for example, three-dimensional images (Ref 1). This technique is available in many microscopes and spectroscopic apparatus and offers important advantages respect to wide-field microscopy, such as the possibility to control the depth of field (Ref 2), a reduction of the background signal coming from regions away from the focal plane and the possibility to collect signals from specific regions of thick samples allowing a 3D reconstruction (Ref 3-5). This technique is extremely popular due to the easiness with which high-quality images can be obtained from samples prepared for conventional fluorescence microscopy; it is widely used in cell biology to study fixed and living cells and tissues (Ref 6-11), or in inhomogeneous materials for morphology characterization (Ref 12-16).

The confocal technique works well when the goal is to obtain or reconstruct an image in two- or three-dimensions of a specimen in the interior of a sample when the material above is transparent enough to allow the incident light get into the region of interest and the scattered light be refracted to the detector.

The Raman technique allows a chemical characterization of samples by determining the vibrational normal modes of their atoms and molecules: an analysis of the light inelastically scattered by the molecules allows the identification of the chemical groups present in the sample. The intensity of the Raman bands depends, among other things, on the number and type of the scatters present in the illuminated volume.

R. Rodriguez, S. Vargas, and **M. Estevez**, Fisica Aplicada y Tecnología Avanzada, UNAM, Campus Juriquilla, Apdo. Postal 1-1010, Querétaro, México. Contact e-mail: rogelior@servidor.unam.mx.

2. Methods

2.1 Confocal Technique

The confocal technique is based on the use of a spatial filter (a lens-pinhole system) where the collected light is focused by the lens on the pinhole placed on the conjugated focal plane. Then, the spatial filter rejects practically all signals coming from objects situated out of the focused region. By changing this, it is possible to observe sections of the sample placed at different depths.

It is claimed that with only a single illuminated point, the illumination intensity rapidly falls off above and below the focal plane as the beam converges and diverges, thus reducing the illumination of objects situated out of the focal plane. Then, this technique allows analyzing precise specimens situated at different depths into the sample. In principle, the aperture will block any light emanating from regions away from the vicinity of the illuminated specimen. Most confocal imaging systems provide adjustable pinhole blocking apertures, enabling a better tradeoff in vertical resolution and sensitivity: a small pinhole gives high resolution but weak signal.

In summary, a confocal imaging system achieves out-of-focus rejection by two strategies: (a) by illuminating a single point of the sample with a highly focused beam, so that illumination intensity drops off rapidly above and below the focal plane and (b) by the use of a blocking pinhole aperture placed in the conjugated focal plane to the specimen so that the light emitted by regions away from the illuminated specimen is blocked from reaching the detector. The confocal imaging can offer an improved resolution of up to 40% relative to a microscope operated conventionally.

2.2 Nonlocal Contributions

When Raman analysis is performed using micro-Raman spectroscopy in confocal mode, the situation is different because the light that arrives the detector passes through the material placed on the top of the specimen; a considerable part of this light, scattered inelastically by molecules in this portion of material (that is off the focal plane), reaches the detector producing a contribution to the Raman spectrum. There is also a contribution from the material placed below the specimen because the incident light also reaches this region is scattered reaching the detector. In Fig. 1, it is possible see a schematic diagram illustrating the laser light focused, by a microscope, in the interior of a inhomogeneous sample; additionally are shown the illuminated cones (upper and lower), the pinhole aperture, the specimen placed in the focal plane, the subcone where the light scattered by molecules in this region is not blocked by the aperture. The incident light illuminates the cones (shady areas) above and below the specimen placed in the focal plane; then part of the light scattered by molecules in these cones is collected by the optics and sent to the detector producing nonlocal, nonnegligible, and nondesirable contributions to the total Raman signal.

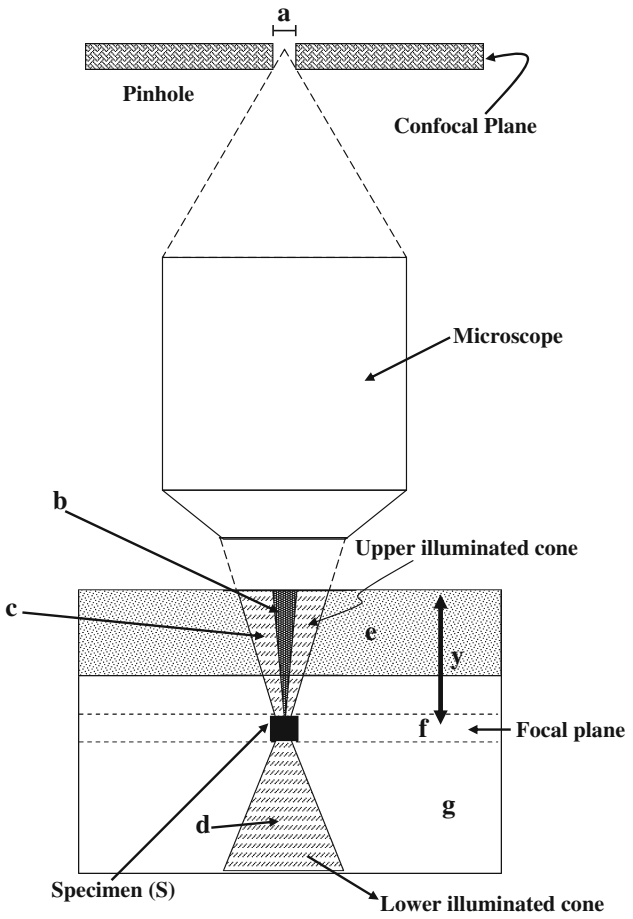

Fig. 1 Schematic diagram illustrating the laser light focused, by the microscope, in the interior of a inhomogeneous sample: (a) the pinhole aperture size and the base of the sub-cone; (b) the subcone, of the upper illuminated cone, with a base of the same size as the pinhole aperture: the light scattered by molecules in this region passes through the pinhole reaching the detector; (c) the upper illuminated cone: only part of the light produced in this region reaches the detector; (d) the lower illuminated cone: only part of the light produced in this region reaches the detector; (e) the upper phase of the inhomogeneous coating; (f) is the focal plane where is placed the specimen (S): all light form the specimen passes through the pinhole reaching the detector; (g) the lower phase of the inhomogeneous coating; and (y) (see Eq 1) the distance from the coating surface to the specimen (focal plane)

These nonlocal contributions are important because the confocal Raman analysis is employed to determine precisely the chemical composition as a function of depth. This nonlocality, unimportant for image analysis (where the only requirement is the transparency of the material on the top of the specimen), can be a serious problem for the confocal Raman analyzes of inhomogeneous systems.

Anti-graffiti coatings and others inhomogeneous materials are important from the technological point of view, then it is important to characterize properly these multiphase materials (Ref 17-21). In this work, a confocal Raman analysis was performed to characterize anti-graffiti coatings.

3. Experimental

3.1 Materials and Synthesis

To determine the impact of these nonlocal effects in the Raman spectra, homogeneous and in-homogeneous materials were analyzed: four alkyd polyurethane anti-graffiti coatings of 35-μm thickness and with different concentrations of antiadherent (0% (homogeneous), 2%, 4%, and 6% (inhomogeneous)) were used. In addition to these coatings, a homogeneous 6-mm thick slab of commercial polymethyl metacrylate (PMMA) (QuimiNet, Rhom and Haas, Mex.) was selected due to its high purity and transparency (negligible absorption in the visible spectrum) and because has a flat surface and a refractive index similar to the alkyd resin, allowing to study the confocal signals when the material's boundary is far from the focused region.

The anti-graffiti coatings were prepared as reported elsewhere (Ref 22): a commercial hydroxylated alkyd resin (Reichhold, Mex) was used as the polymeric base, the crosslinking agent was polyisocyanate (Bayer, Ger), the antiadherent was polysiloxane (Degussa, Ger.) and the organic solvent was toluene (Baker, USA). Ten grams of alkyd resin were mixed, at room temperature during 10 min, with 6.0 g of toluene and with the corresponding amount of polysiloxane. Separately, the 2.5 g of polyisocyanate were mixed with 3.0 g of toluene. These two blends were mixed together during 5 min; a cloudy appearance was obtained due to the segregation effects. A high shear rate propel must be used during this mixing process to reduce the particle size of the aggregates. At these conditions, the final mixture takes about 3 h to become superficially dry. Once the final mixtures were prepared, they were immediately brushed on flat pieces of silicon wafers obtaining thicknesses of (35 ± 5) μm. All coatings were cured during 5 days at room temperature to allow finish completely the chemical reaction. The solvent provides enough mobility to the antiadherent (AA) molecules to produce the phase separation during the curing time. When the chemical reaction has finished, an inhomogeneous coating was obtained where the AA molecules are mainly placed on the external (exposed) surface.

3.2 Characterization

For all materials, the Raman spectra were obtained using a Dilor Micro-Raman Spectrometer model Labram operated in the confocal mode at room temperature (25 °C). The light source was a He-Ne laser (λ = 632.8 nm) of 5 mW and a 50× objective with a numerical aperture of 0.75 and a pinhole of 200 μm; the estimated illuminated volume in the sample for 30 μm depth was 30 mm^3. The observed wavenumber region was from 500 to 3000 cm^{-1}.

Series of Raman spectra were taken in the confocal mode from the surface to 200 μm deep for the acrylic plate and to 30 μm deep for the coatings; in all cases, a Raman spectrum was taken every 2 μm in depth. The parameters of the spectrometer (laser power, filters, apertures, etc.) were kept unchanged in all cases to compare the bands height as a function of the depth and the concentration of AA.

4. Results and Discussion

To characterize the phase separation, the laser light was focused at different depths inside the sample with the aim to determine the chemical composition as a function of the depth. When a material is analyzed with the confocal μ-Raman technique, the contributions to the spectrum are from molecules at three different regions: the main contribution is from molecules in the focused region because it is where the light energy density reaches its highest value and the pinhole in the confocal plane does not produce any blocking of this signal (Fig. 1). The next contribution is from molecules in the upper illuminated cone above the focused region (near the objective) because the light energy density is lower, the optical path of the scattered light is shorter, and there is a partial blocking of the signal by the pinhole. The last contribution is from molecules in the cone below the focused region; this contribution is less significant respect to the former one because the energy density is even lower, the optical path is larger and also suffers a partial blocking by the pinhole. This is illustrated in Fig. 1 where the layers of the inhomogeneous coating are shown together with the rays coming from different parts of the illuminated sample.

To quantify these effects, homogeneous (PMMA slab and a 0% AA coating) and inhomogeneous (2%, 4%, 6% AA coating) samples, were analyzed. If the contribution to the spectrum was only due to the molecules in the focused region, the band intensities should be practically constant as the laser light was focused deeper into the homogeneous materials. In Fig. 2, it is possible to see a series of Raman spectra taken at different depths into the acrylic slab. As can be seen, not only the intensities of practically all bands changed with the depth, but also some new bands appeared: 1215 and 1486 cm^{-1}. When the laser was focused on the surface (0 μm depth), the signal that reached the detector had low intensity, essentially because there was not upper illuminated cone. However, when the laser light was focused deeper, the upper illuminated cone grew in size and more light coming from it reached the detector increasing the bands intensities. Then when a chemical analysis is required for some particular region into the sample, the confocal μ-Raman setup introduces nonlocal contributions to the spectra from regions nearby the region of interest; these effects have to be taken into account for a correct interpretation of the spectra and a correct determination of the segregated phase.

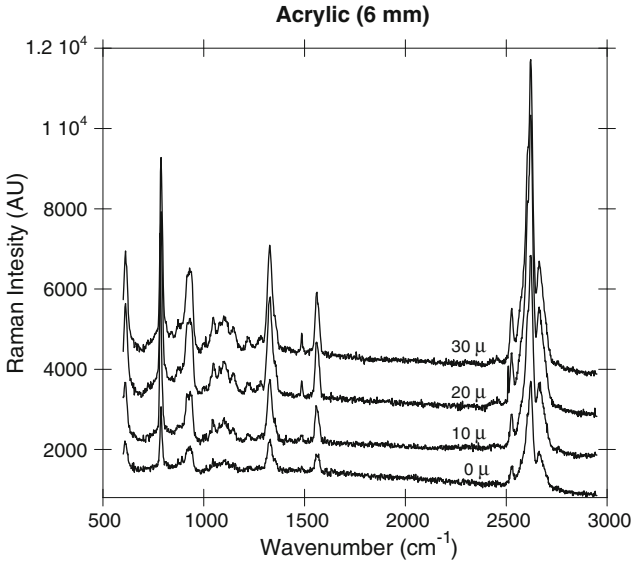

Fig. 2 Set of Raman spectra taken at different depths in a 6 mm thick acrylic commercial plate

In Fig. 3(a) and (b), it is possible to see the bands heights as a function of depth for PMMA. As can be seen the intensities of these bands grew between 300% and 560% as the laser was focused deeper into the slab. This behavior (referred as regime 1) is typical for homogeneous materials, and is due to an increment in the volume of the illuminated cone, i.e. to an increment in the number of molecules that scatter light to the detector. The illuminated volume is defined as the intersection of the cone light subtended by the microscope objective and the sample itself. As the cone angle θ is constant (Fig. 1), the volume of the illuminated cone increases cubically with the depth "y": $\mathrm{Vol} = \left(\frac{1}{3}\pi tg^2(\theta)\right)y^3$.

Based on this equation, the band height (BH) can be modeled as:

$$\mathrm{BH} = a(y+b)^3 + c, \qquad \text{(Eq 1)}$$

where the parameter a, which provides the intensity of the Raman bands, depends on the apparatus geometry and the quantum efficiency of the radiation absorption, b is related to the reference in the depth measurement, and c is the baseline. Figure 3(b) shows the fitting (the continuous lines) of the bands heights for some bands using Eq 1; as can be noticed the data were well fitted with this equation.

The subcone shown in Fig. 1 has a base of the same size as the pinhole aperture; the light scattered by molecules in this region passes through the pinhole reaching the detector without any blocking. For deeper penetrations, the volume of the illuminated cone becomes larger than the sub-cone, producing that part of the scattered light coming from molecules in this region was blocked by the pinhole and could not reach the detector; only molecules in the subcone produce scattered light that has contribution to the Raman spectra. For this reason the bands heights remained practically constant (regime 2); in this particular case, the regime 2 was reached for depths larger than 20 μm. When the incident light was focused deeper than 30 μm, the bands heights were reduced (not shown) due to an increment in the optical path of the scattered light, producing a reduction in the intensity that reaches the detector (regime 3).

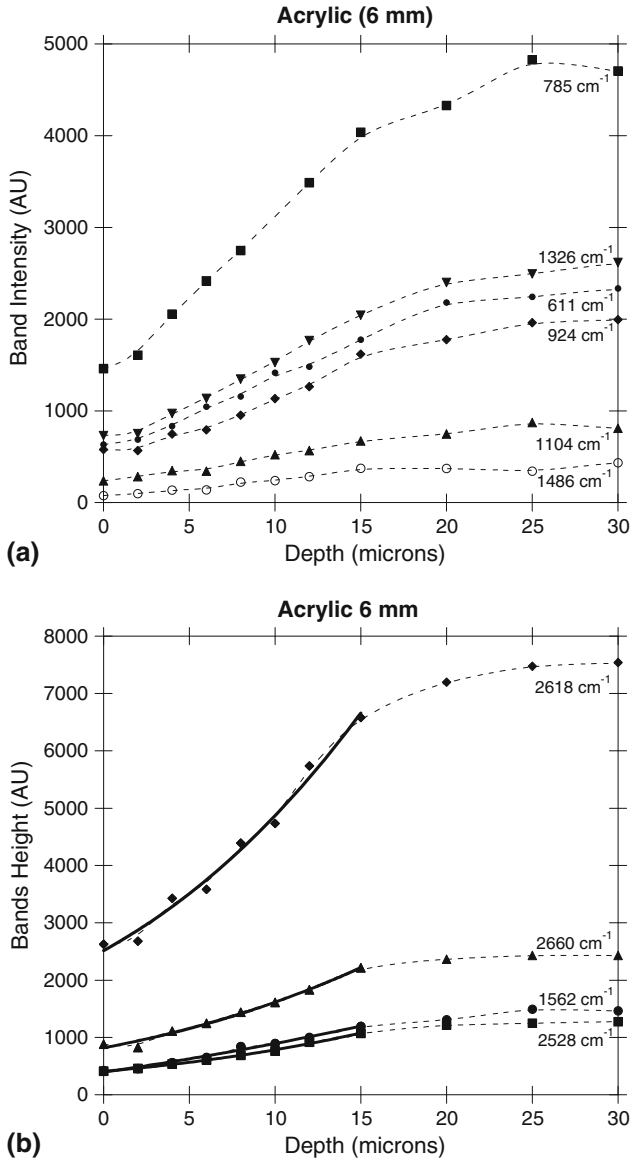

Fig. 3 (a) Some bands heights profiles for PMMA sample; (b) Fitting of the heights profiles of some other bands for PMMA sample: the continuous lines correspond to a fitting using the model reported in Eq 1

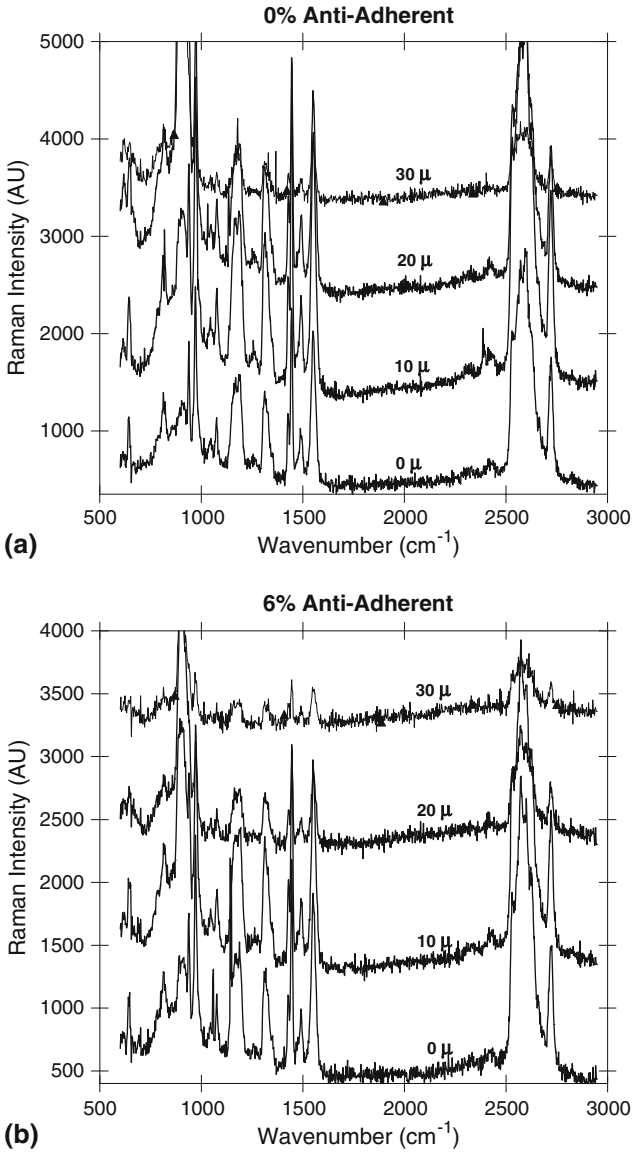

Fig. 4 Set of Raman spectra at different depths for the coating with (a) 0% AA and (b) 6% AA

Figure 4(a) and (b) shows the Raman spectra of the coatings containing 0 and 6% of AA; the other samples show similar behavior. The bands heights of these spectra are reported in Fig. 5 (0% AA) and 6 (6% AA). Because the coating with 0% AA is a homogeneous material, the intensity profiles (Fig. 5) had essentially the same initial behavior as for the PMMA (Fig. 3a and b): the bands intensity for low penetrations grew cubically with the depth for the first 10 µm (regime 1) and for deeper penetrations the bands heights remained practically constant (regime 2). After this regime, the bands heights were reduced reaching low values for depths near 30 µm (regime 3). In this case, the reduction in the bands intensities was considerable not only by the increment in the optical path, but also due to the low thickness of the sample (35 µm): the proximity to the coating boundary reduced significantly the lower illuminates cone and consequently the light that reached the detector; additionally the light absorption effects also produced important reduction in the intensity.

When the 6% AA coating sample was analyzed (Fig. 6), the heights profiles were different: they did not show the regime 1 characterized by an increment in the bands heights with the depth in the first microns near the surface, but instead they remained practically constant (regime 2), decaying to low values for deeper penetrations (regime 3). The absent of the regime 1 at the beginning of the profiles means that this coating is essentially different, at least near the surface, to the other analyzed samples; this is indicative of the phase separation. It has been demonstrated (Ref 22) that, for the anti-graffiti, the AA deposits on the external surface, becoming an inhomogeneous coating. To suppress the regime 1 and to obtain instead a regime 2, the AA must be distributed into the coating following a decreasing gradient from the surface to the interior. For compensation, the PU (the other coating component) must also follow an increasing gradient form the surface to the interior. In this way, the increment in intensity produced by an increase in the volume of the illuminated cone is compensated negatively

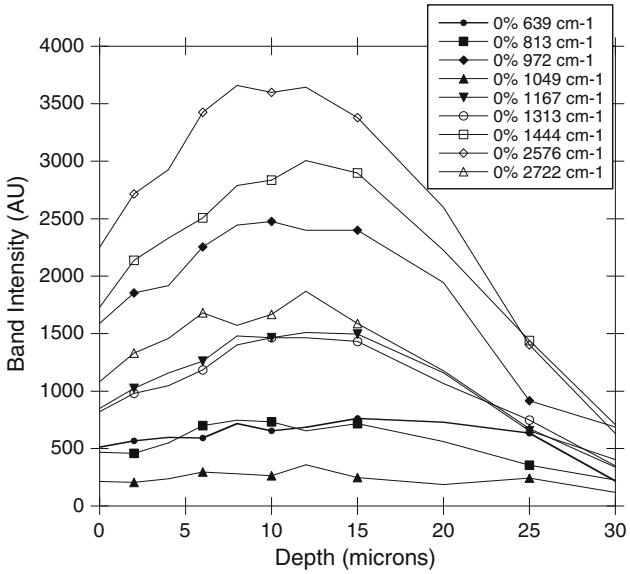

Fig. 5 Bands heights profiles for the 0% AA coating

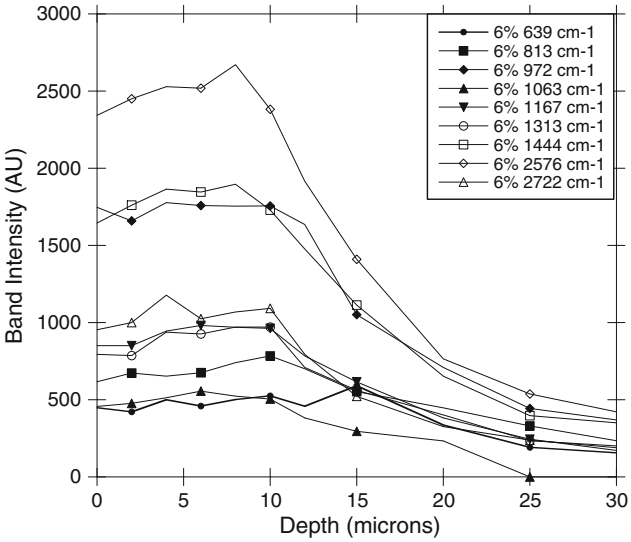

Fig. 6 Bands heights profiles for the 6% AA coating

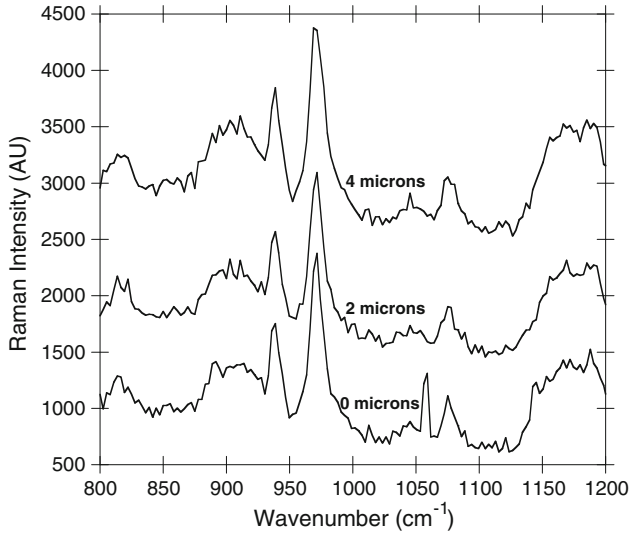

Fig. 7 Detail of Raman spectra at different depths for the 6% AA coating

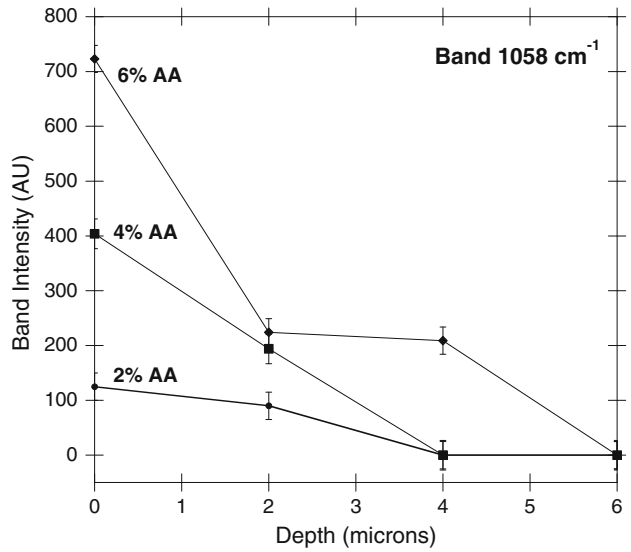

Fig. 8 Heights of the 1058 cm^{-1} band as a function of depth for the 6% AA coating

by a reduction in the number of molecules due to the decreasing concentration gradient.

This assumption was supported by the results reported in Fig. 7 and 8. Figure 7 shows a detail of the Raman spectra for the 6% AA sample where it is possible to observe a defined band at 1058 cm^{-1} that reduces rapidly to zero when the depth is increased; this band corresponds to the stretching vibration of the Si-O-Si group that is the structural unit of AA. Figure 8 shows the band height for the band at 1058 cm^{-1} as a function of the depth for samples with 2%, 4% and 6% AA. As can be noticed, the AA was distributed in a layer from 4 to 6 μm following a decreasing concentration gradient; after 6 μm depth there was not AA present in the coating (only PU). Figure 9 shows a comparative between the bands heights for PU and for AA. Here it is possible to see that, while the AA the profiles were reduced (a decreasing gradient), the PU profiles were incremented (increasing gradient) for compensation. These results can be used to characterize inhomogeneous materials where one phase is segregated to the surface: if the bands heights remain practically constant in the first microns deep into the film, this corresponds to an inhomogeneous coating; on the other hand, if the bands heights grow (cubically) with penetration, the film is homogeneous.

5. Conclusions

It was possible to analyze homogeneous and inhomogeneous materials using confocal Raman spectroscopy. They showed different bands heights profiles near the external surface: while for homogeneous materials the bands heights

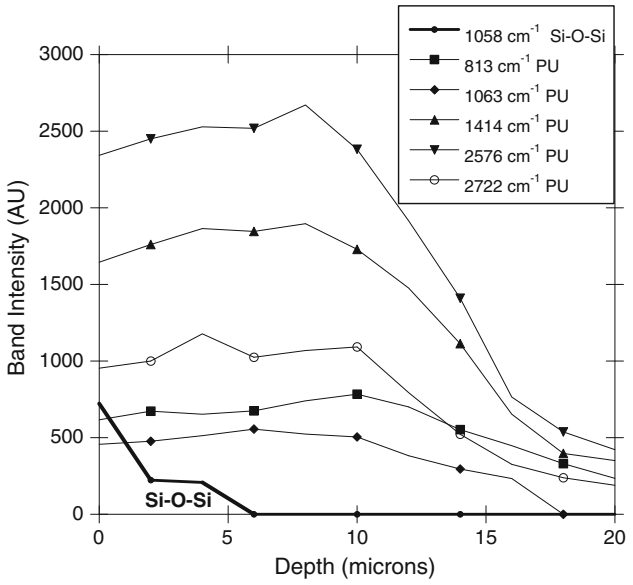

Fig. 9 A comparison between the PU bands height and the 1058 cm^{-1} band of 6% AA coating

grew cubically with the depth due to an increment in the volume of the illuminated cone, for the inhomogeneous material the bands heights remained practically constant near the surface because the effect produced by the increment in the volume of the illuminated cone was compensated negatively by a decreasing gradient in concentration of the AA phase and by an increment in the optical path. These nonlocal effects were produced because the signal that reaches the detector has contributions not only from the molecules in the focused region, but also from those in the illuminated cones above and below this spot. These nonlocal effects allowed the characterization of a layer-structured coating that is of great technological importance.

Acknowledgment

The authors are indebted to Ing. Francisco Rodriguez Melgarejo by his valuable help in the Raman technique.

References

1. A. Belu, C. Mahoney, and K. Wormuth, Chemical Imaging of Drug Eluting Coatings: Combining Surface Analysis and Confocal Raman Microscopy, *J. Control. Release*, 2008, **126**, p 111–121
2. B. Marton, L.G. van Derven, C. Otto, N. Uzunbajakava, M.A. Hempenius, and G.J. Vancso, A Depth-Resolved Look at the Network Development in Alkyd Coatings by Confocal Raman Microspectroscopy, *Polymer*, 2005, **46**(25), p 11330–11339
3. M. Pastorczak, M. Wiatrowski, M. Kozanecki, M. Lodzinski, and J. Ulanski, Confocal Raman Microscopy and 3-Dimencional Shape and Composition Determination of Heterogeneous Systems, *J. Molec. Struct.*, 2005, **744-747**, p 997–1003
4. W. Smitthipong, R. Gadiou, L. Vidal, P. Wagner, and M. Nardin, 3D Raman Images of Rubber Blends (IR-HNBR), *Vib. Spectrosc.*, 2008, **46**(1), p 8–13
5. T. Wermelinger, C. Borgia, C. Solentharler, and R. Spolenak, 3-D Raman Spectroscopy Measurements of the Symmetry of Residual Stress Fields in Plastically Deformed Sapphire Crystals, *Acta Mater.*, 2007, **55**(14), p 4657–4665
6. G.J. Puppels, C. Otto, and J. Greve, Confocal Raman Microspectroscopy in Biology: Applications and Future Developments, *TrAc Trend Anal. Chem.*, 1991, **10**(8), p 249–253
7. Y. Hu, A. Shen, T. Jiang, Y. Ai, and J. Hu, Classification of Normal and Malignant Human Gastric Mucosa Tissue with Confocal Raman Microscopy and Wavelet Analysis, *Spectrochem. Act A Molec. Biomol. Spectrosc.*, 2008, **69**(2), p 378–389
8. C. Scalfi-Happ, A. Jauss, W. Ibach, O. Hollricher, S. Fulda, C. Hauser, R. Steiner, and A. Rück, Confocal Raman Microscopy as a Diagnostic Tool for Investigation of Living Neuroblastoma Tumour Cells, *Med. Laser Appl.*, 2007, **2**(3), p 157–164
9. C. Yu, E. Gestl, K. Eckert, D. Allara, and J. Irudayaraj, Characterization of Human Breast Epithelial Cells by Confocal Raman Microspectroscopy, *Cancer Detect. Prevent.*, 2006, **30**(6), p 515–522
10. A.G. Shen, Y. Ye, Y.W. Zhang, X.H. Wang, J.M. Hu, W. Xie, and J. Shen, Screening of Gastric Carcinoma Cells in the Human Malignant Gastric Mucosa by Confocal Raman Microscopy, *Vib. Spectrosc.*, 2005, **37**(2), p 225–231
11. K. Nithipatikom, M.J. McCoy, S.R. Hawi, K. Nakamoto, K.F. Adar, and W.B. Campbell, Characterization and Application of Raman Labels for Confocal Raman Microspectroscopic Detection of Cellular Proteins in Single Cells, *Anal. Biochem.*, 2003, **322**(2), p 198–207
12. V. Ferreiro, C. Depecker, J. Laureyns, and G. Coulon, Structure an Morphologies of Cast and Plastically Strained Polyamide 6 Films as Evidence by Confocal Raman Microspectroscopy and Atomic Force Microscopy, *Polymer*, 2004, **45**(17), p 6013–6026
13. M.H. Chou, S.B. Liu, C.Y. Huang, S.Y. Wu, and C.L. Cheng, Confocal Raman Spectroscopic Mapping Studies on a single CuO Nanowire, *Appl. Surf. Sci.,* 2008, **254**(23), p 7539–7543
14. A. Kuzmin, R. Kalendarev, A. Kursitis, and J. Purans, Confocal Spectromicroscopy of Amorphous and Nanocrystalline Tungsten Oxide Films, *J. Non-Cryst. Solid*, 2007, **353**(18-21), p 1840–1843
15. M. Österberg, U. Schmidt, and A.S. Jääskeläinen, Combining Confocal Raman Spectroscopy and Atomic Force Microscopy to Study Wood Extractives on Cellulose Surfaces, *Coll. Surf. A Physicochem. Eng. Aspect*, 2006, **291**(1-3), p 197–201
16. O.S. Fleming, S.G. Kazarian, E. Bach, and E. Schollmeyer, Confocal Raman Study of Poly(Ethylene Terephthalate) Fibres Dyes in Supercritical Carbon Dioxide: Dye Diffusion and Polymer Morphology, *Polymer*, 2005, **46**(9), p 2943–2949
17. S.J.F. Erich, J. Laven, L. Pel, H.P. Huinink, and K. Kopinga, Comparison of NMR an Confocal Raman Microscopy as Coatings Research Tools, *Prog. Org. Coat.*, 2005, **52**(3), p 210–226
18. P.D.A. Pudney, T.M. Hancewicz, D.G. Cunningham, and M.C. Brown, Quantifying the Microstructure of Soft Solid Materials by Confocal Raman Spectroscopy, *Vib. Spectrosc.*, 2004, **34**(1), p 123–135
19. L. Baia, K. Gigant, U. Posset, R. Petry, G. Schottner, W. Kiefer, and J. Popp, Confocal Raman Investigations on Hybrid Polymer Coatings, *Vib. Spectrosc.*, 2002, **29**(1–2), p 245–249
20. F. Magistro, D. Majolino, P. Migliardo, R. Ponterio, and M.T. Rodriquez, Confocal Raman Spectroscopic Study of Painted Medieval Manuscripts, *J. Cult. Herit.*, 2001, **2**(3), p 191–198
21. C. Fagnano, M. Rpssi, R.S. Porter, and S. Ottani, A Study on Solid-State Drawn Fibers of Polyethylene by Confocal Raman Microspectrometry: Evaluation of the Orientation Profiles of Amorphous and Crystalline Phases Across the Fiber Section, *Polymer*, 2001, **42**(13), p 5871–5883
22. R. Rodriguez, S. Jimenez-Sandoval, M. Estevez, and S. Vargas, Drying Kinetics and Segregation in a Two-Component Anti-Adherent Coating Studied by Photoluminescence and Raman Spectroscopies, *J. Non-Cryst. Solids*, 2008, **354**(30), p 3623–3629